CFD simulation for opaque ventilated facades in hot arid climate based on literature review design parameters.

Ahmed Alyahya[1,2], Simon Lannon[1], Wassim Jabi[1]
[1]Cardiff University, Cardiff, United Kingdom
[2]Imam Abdulrahman Bin Faisal University, Dammam, Saudi Arabia

Abstract

In this paper, computational fluid dynamics (CFD) simulations were conducted to analyse the design parameters found in the literature review that influence the performance of an opaque ventilated façade (OVF) and provide a baseline prototype for future parametric optimisation of novel OVFs. The baseline prototype is created by combining the most common OVF geometrical solutions discovered in the literature and applied in Riyadh, Saudi Arabia, which is an extremely hot and arid region. The CFD simulation results indicate that airflow velocity within the OVF's cavity has the most significant effect on its thermal performance in hot, arid climate areas.

Highlights

- Increasing the airflow velocity inside the cavity can lead to a 6°C reduction in the inner skin surface temperature.
- Shading the OVF can lead to a 4.1°C reduction in the inner skin surface temperature.
- Changing the OVF's outer skin material can lead to a 3.3°C reduction in the inner skin surface temperature.
- Closing the OVF's joint configuration can lead to a 2.1°C reduction in the inner skin surface temperature.
- Adjusting the cavity width can lead to a 0.9°C reduction in the inner skin surface temperature.

Introduction

Over the past few years, opaque ventilated façades (OVF) have become increasingly popular as an envelope solution for a wide variety of building types and climates (Ibañez-Puy et al., 2017). In the literature, OVFs are described in many different terms, including ventilated façade, ventilated wall, opaque double-skin façade, ventilated curtain wall, and rainscreen wall. The OVF consists of two opaque layers separated by a ventilation channel, with its outer skin usually constructed of composite panels with either closed or open joints, as seen in Figure 1 (Ibañez-Puy et al., 2017).

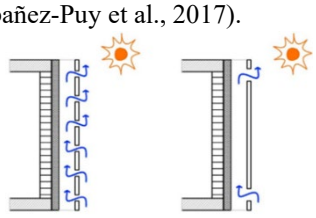

Figure 1: Open joints ventilated façade (left) and closed joints (right) (Ibañez-Puy et al., 2017).

OVFs are popular among architects for a number of reasons, including their ability to be customised with materials, colors, and shapes. Apart from their aesthetic qualities, exterior cladding layers are also extremely fast and easy to install (Sanjuan et al., 2011). Moreover, both new buildings and façade renovations can make use of an OVF system (Sarihi et al., 2021). It has also been shown that OVFs can reduce the heat flux into the building envelope during the summer, allowing a 20% to 55% savings in energy consumption (Fantucci et al., 2020; Gagliano & Aneli, 2020; Ibañez-Puy et al., 2017; Maciel & Carvalho, 2019). OVF systems can also reduce condensation and infiltration during the winter, extending the durability of the façade (Fantucci et al., 2020).

Simulating the façade's performance plays a key role in evaluating OVFs. Computational Fluid Dynamics (CFD) simulations can determine the temperature of the façade surfaces inside and outside the cavity in order to predcit the reduction of the OVF's heat gain. CFD is "a science that, with the help of digital computers, produces quantitative predictions of fluid-flow phenomena based on the conservation laws (conservation of mass, momentum, and energy) governing fluid motion" (Hu, 2012, p. 421). CFD code explores the relationship between velocity, pressure, temperature, and density by solving the Navier-Stokes Equations (McLean, 2013).

This study required a careful selection of a CFD simulation software. Table 1 show the CFD software and settings used in recent OVF research, highlighting the time averaging calculations used to solve the Navier-Stokes equations, a description of the geometry model of each study, and the models that utilise the Navier-Stokes equations, are displayed. Ansys Fluent (ANSYS, 2022) was used in the majority of these studies, which has been validated by performing numerical analyses and experimental comparisons which show a good correlation between CFD results and experimental data (Buratti et al., 2018; Sánchez et al., 2020; Sotelo-Salas et al., 2021).

Models based solely on conduction and/or convection are the simplest, whereas models like an OVF, which are based on buoyancy-driven flow and natural convection and flow involving radiation, are more complicated. According to Gagliano and Aneli (2020), OVF performance should be calculated through a transient analysis and not through a steady-state calculation. Although this technique has strong potential for practical applications, it requires excessive computational

resources to obtain valuable information about the performance of OVFs (Stavrakakis et al., 2008). Some studies in Table 1 have used the steady state method to overcome these technical difficulties. With the aid of experimental measurement data, these studies validated the steady state application's ability to solve Navier-Stokes equations in OVF (Buratti et al., 2018; C. O. Souza et al., 2018; Sánchez et al., 2020; Sotelo-Salas et al., 2021). To overcome the steady state challenge, some research employed the pseudo transient method, where the steady state equations are given an artificial time derivative to increase stability and convergence (Ferziger et al., 2020). This means that for each fluid zone and solid zone, a separate time step size can be defined in the run calculation under Pseudo time settings (ANSYS, 2022).

Regarding the turbulence model, nearly all of the studies in Table 1 used the k-epsilon (k-ε) turbulence model to investigate the effects of turbulence. Sánchezet al.(2020) carried out a comparison of the turbulence models to see which one was most in line with the experimental findings. They discovered in their study that the renormalization group (RNG) k-ε (Yakhot & Orszag, 1986) aligns the simulated and experimental data more precisely. Additionally, several studies agreed that the RNG k-ε model is recommended for good results and also for good simulation stability (Castillo et al., 2019; Pasut & De Carli, 2012; Stavrakakis et al., 2008).

Turbulent flows are substantially impacted by the presence of walls. The quality of numerical solutions is significantly impacted in near-wall modelling when walls are the primary source of turbulence and vorticity. Some studies recommended choosing the two-layer for the enhanced wall treatment in order to more accurately describe the near-wall region for the k-ε model (Pasut & De Carli, 2012; Teodosiu et al., 2014).

Some of the studies in Table 1 did not specify the radiation model that was employed since they did not show a comprehensive CFD setup. Nonetheless, the discrete ordinates (DO) model was employed by the vast majority of the studies. To determine the most appropriate radiation model to simulate OVF, Sánchez et al. (2020) examined various radiation models with actual experimental measurements. It was discovered that the DO model provides a more precise prediction of how these façades will perform against solar radiation.

Through this study, the design parameters found in the literature review that affect the performance of an OVF will be modelled and simulated by CFD in a hot arid climate to create a baseline façade for future parametric optimisation. To date, this approach has not been used to show in detail the most effective design parameter that affects the performance of an OVF in a hot arid climate. The techniques described can be used to explore other OVF designs as part of an ongoing study. Therefore, this study highlights which parameters should be taken into consideration when designing a novel OVF to reduce heat gain in hot arid regions.

Table 1: Previous numerical studies on OVF.

Author/year	Geometry model	CFD software	Navier Stokes calculation	Turbulence model	Radiation model
(Gagliano et al., 2016)	A ventilated façade with 6m height and 0.15m air cavity.	Ansys Fluent	Transient	RNG k–ε	DO
(Astorqui & Porras-Amores, 2017)	A ventilated façade with 10m height and 0.11m air cavity.	STAR-CCM+	Steady state	Realizable k–ε	DO
(Lai & Hokoi, 2017)	A ventilated BIPV wall with 1.3m height, 0.5m width and 0.05 to 0.2 m air cavities.	PHOENICS	Not mentioned	k–ε	Not mentioned
(C. O. Souza et al., 2018)	A test cell with 3.05 × 3.50m, 3.0m height and 0.10m air cavity.	Ansys CFX	Pseudo steady state	k–ε	Not mentioned
(Buratti et al., 2018)	A ventilated façade with 2.52m height and 0.08m air cavity.	Ansys Fluent	Steady state	Standard k–ε	P1
(Sotelo-Salas et al., 2019)	A test cell with 3×3×3m and the air cavity ranging from 0.1 to 0.5m.	Ansys Fluent	Steady state	Not mentioned	Not mentioned
(Gagliano & Aneli, 2020)	A ventilated façade with 6m height and 0.15m air cavity.	Ansys Fluent	Transient	RNG k–ε	DO
(Schabowicz & Zawiślak, 2020)	A ventilated façade with 4m height and 0.05m air cavity.	Ansys Fluent	Not mentioned	RNG k–ε	DO
(Sánchez et al., 2020)	A ventilated wall with 0.825m height, 1.225m width and 0.045m air cavity.	Ansys Fluent	Pseudo steady state	RNG k–ε	DO
(Sotelo-Salas et al., 2021)	A test cell with 3×3×3m and the air cavity ranging from 0.2 to 1 m.	Ansys Fluent	Steady state	Realizable k–ε	Not mentioned
(Schabowicz et al., 2021)	A ventilated façade with 4m height and 0.05m air cavity.	Ansys Fluent	Not mentioned	RNG k–ε	DO
(Nghana et al., 2021)	A ventilated façade with 2.2m height and 0.013m air cavity.	STAR-CCM+	Transient	Standard k–ε	DO

Methodology

The most common geometrical solutions for OVF in hot climates found in the literature were tested by Ansys Fluent on a test cell in Riyadh, Saudi Arabia, which is an extremely hot and arid region. August was chosen because it is the hottest month of the year in Saudi Arabia. The OVF was oriented east to simulate the peak temperature a façade might reach. In the literature review, geometric solutions include the dimensions of the test cell, the width of the ventilated cavity, and the material and joint configuration of the outer skin.

Various design solutions were found in the research literature; however, most of them have some geometrical similarities, such as a test cell dimension of 3 × 3 × 3m which is selected to determine the test cell size (C. O. Souza et al., 2018; Coma et al., 2017; Sotelo-Salas et al., 2019, 2021). There are several different options for the width of the ventilated cavity found in the literature. According to several studies, cooling occurs for cavities larger than 7 cm, and energy savings are improved as air chamber widths increase, especially for cavities wider than 15 cm (Balocco, 2002; M. Ciampi et al., 2003). However, when the cavity width is increased to 35 cm, the cooling effect becomes stable (Balocco, 2002). Therefore, 5, 10, 20, and 30 cm air cavity widths were tested in this study.

Four materials were tested for the outer skin: glass-fibre reinforced concrete panels, aluminium, autoclaved-aerated concrete panels, and PVC-coated polyester fabric. The outer skin options are listed in Table 2, along with their density (kg/m3), thermal conductivity (W/m/K) and specific heat capacity (J/kg/K). Figure 2 includes the test cell details as well as the parameters tested in this study to create the baseline ventilated façade and find the most effective design parameters for the façade.

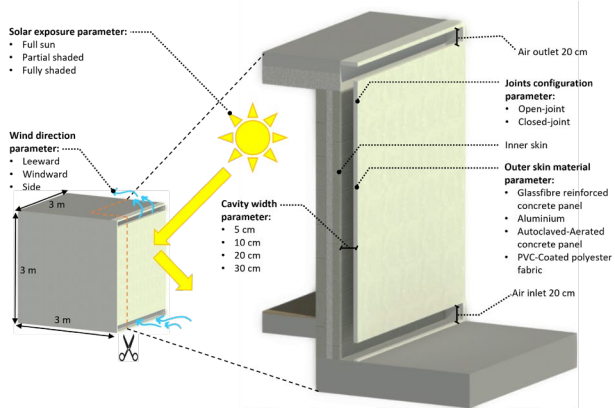

Figure 2: The test cell details and the tested parameters to create the baseline ventilated façade.

Table 2: Properties of the test cell outer skin materials.

Material	Thickness (cm)	Density (kg/m³)	Thermal conductivity (W/m/K)	Specific heat capacity (J/kg/K)
Glassfibre reinforced concrete[1]	1.3	2000	2	1000
Aluminium[2]	0.1	2719	202.4	871
Autoclaved-Aerated concrete[3]	5	565	0.129	1035
PVC-Coated polyester fabric[4]	0.095	579	1.64	1000

1- (Rieder, 2017). 2- Fluent database materials.
3- (Sotelo-Salas et al., 2021). 4- (G. Ciampi et al., 2021).

CFD setup

Several steps were followed in the numerical study using Ansys Fluent in the Ansys Workbench module. As a first step, the models were built in three dimensions using Ansys SpaceClaim. This is followed by generating the mesh using Ansys fluent watertight meshing workflow. After that, turbulence and radiation models, boundary conditions, and pressure-velocity coupling solution methods were defined in the fluent solution. Finally, the results were displayed using Ansys CFD Simulation Post Processing.

An extended domain surrounding the building was created, as shown in Figure 3, to capture all flow motions. An unstructured polyhedral mesh was used to discretize the near wall. The size of the grid gradually increased from the finer grids in the air cavity to the rest of the domain by specifying the minimum and maximum mesh elements and surface growth ratio. To ensure that the mesh density is sufficient to capture the desired phenomena while keeping computational costs to a minimum, a grid independence analysis was conducted. Several mesh sizes were used on the cavities, varying in range from coarse mesh (130 k) to the finest mesh (820 k) cells, to verify the grid independence. A comparison of the average air velocity results for these meshes inside the cavity is shown in Figure 4. The results illustrate that all medium, fine, and very fine meshes were in good agreement. Thus, the medium mesh (320k) cells was selected. The medium mesh is suitable for accurate calculations in the boundary layer zones, and the model was numerically verified for accuracy. For computation, mesh sizes that resolve the log-law region (fully turbulent), whose y+ value is between 30 and 60, are sufficient without requiring further refinement into the viscous layer (Salim & Cheah, 2009). The wall y+ is a non-dimensional distance, like local Reynolds number, that is used in CFD to define how coarse or fine a mesh is for a given flow (Salim & Cheah, 2009). All walls met this requirement, with y+ values averaging 30. This was applied to almost all cases except the open-joint OVF due to the small size of the joints, which required a finer mesh with 3 million cells.

Next, a computational volume mesh was generated to cover the entire domain of the flow. In Ansys, the volume mesh was switched to a fluent solution. At steady state,

Reynolds-averaged Navier-Stokes equations (RANS) were used to simulate the flow. The conservation equations for mass, momentum, and thermal energy were used to predict temperature and velocity in the field.

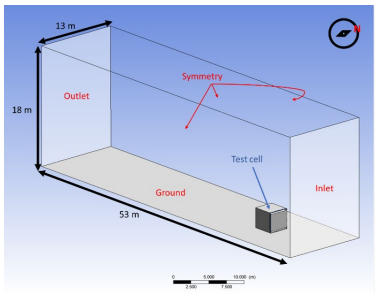

Figure 3: The computational domain.

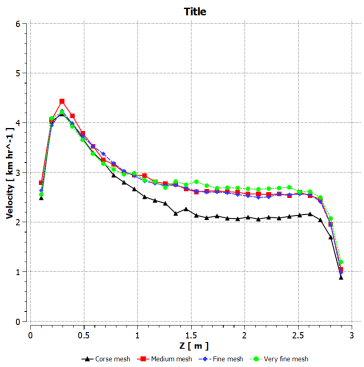

Figure 4: Comparison of vertical velocity profile.

The RNG k-turbulence model was chosen, and the enhanced wall treatment was enabled. To model buoyancy effects, gravitational acceleration forces were included in the momentum equation using the Boussinesq approximation (Ferziger et al., 2020; Gray & Giorgini, 1976). Regarding the radiation model, the DO radiation model was selected. In the boundary conditions, the air temperature was assumed to be 45ºC, and the wind speeds were on three variants of air inflow: 5, 10, and 20 km/h, representing a calm breeze, a light wind, and a moderate wind. Additionally, each wall surface material, thickness, thermal condition, and emissivity were determined based on their physical properties.

The last step before running the CFD simulation was to set up the solution and the calculation tasks. Pressure–velocity coupling was implemented using a coupled scheme. In all equations, second order discretization has been used. CFD model numerical convergence was determined by identifying target scaled residuals at a value of 10^{-3} for X, Y, and Z momentum, continuity, and k, ε equations, 10^{-6} for energy and radiation equations, as recommended by several studies (Gagliano & Aneli, 2020; Pasut & De Carli, 2012). Furthermore, another convergence factor has been considered, which is to set field monitors for temperature and cavity airflow velocity during simulation runtime until these values remain consistent and do not fluctuate.

Discussion and results

The study examined several façade parameters, including outer skin materials, air cavity width, joint configuration, wind direction and velocity, and solar exposure. Based on CFD simulation data, a sensitivity analysis was conducted to identify the façade features most effective for summer thermal performance. The reduction in surface temperature was evaluated as a measure of thermal performance.

Outer skin materials and the wind velocity parameter

A material's properties determine whether solar radiation is reflected or absorbed when it reaches the outer skin. Table 3 shows the CFD results for four outer skin material scenarios under three different wind conditions: a calm breeze, a light breeze, and a moderate breeze. Glass fibre reinforced concrete panels, aluminium and PVC-coated polyester fabric responded almost identically to wind-speed scenarios on the inner skin surface and average air temperature. However, the autoclaved-aerated concrete panel reduced the average temperature better, both on the inner skin surface and in the air inside the cavity, as illustrated in Table 3.

A 5 km/h wind velocity caused the inner skin surface temperature to reach 62.7ºC when using autoclaved-aerated concrete as an outer skin. This is 3.3ºC lower than the aluminium, and PVC-coated polyester fabric outer skin scenarios, which had the worst effect on inner skin temperature reduction. The difference between them was 2.8°C at 10 km/h and 2.0°C at 20 km/h wind. Thus, the effect of the outer skin material type on the inner skin surface temperature decreases as the air velocity inside the cavity increases from 2 km/h during a calm breeze to 5 km/h during a moderate wind. It has also been found that changing the outer skin material type had a negligible influence on the average airflow speed inside the cavity at each wind velocity.

The CFD simulation results also show that airflow velocity inside the cavity had a significant impact on inner skin surface temperature. Figure 5 shows 3D pictures of the test cells with the outer skin hidden to show wind velocity's effect on the inner skin in the autoclaved-aerated concrete panel outer skin scenario, since it contributed the most to lowering the inner skin surface temperature. Furthermore, the figure displays section graphs showing the air temperature distribution and airflow velocity in the middle of the cavities. Inner skin temperature was 2.4ºC lower when wind speed increased from 5 to 10 km/h and 6.0ºC lower when wind speed increased from 5 to 20 km/h. Therefore, it can be seen that increasing the airflow speed inside the cavity provides almost double the effect of changing the outer skin material type on the surface temperature of the inner skin.

Joints configuration parameter

The air flow through the cavity is determined by the outer skin's configuration, which can be open or closed. The upward flow is continuous, homogenous, and symmetrical along the wall in the case of closed joints, where the air inlet is at the bottom and the outlet is at the top of the outer skin. On the other hand, the airflow in an open joint OVF is significantly more complicated, inhomogeneous, and asymmetrical, as seen in Figure 6, which shows the airflow streamlines through the cavity at

all simulated wind speeds and their impact on the inner skin surface temperature.

Table 3: The CFD simulation results for the outer skin materials and wind velocity parameters.

Variables		Inner skin temperature	Average air temperature inside the cavity	Average air velocity inside the cavity
Wind velocity	Outer skin material			
(5 km/h) Windward	Glassfibre reinforced concrete panel	65.8 ° C	49.7 ° C	2.0 km/h
	Aluminium	66.0 ° C	49.7 ° C	2.0 km/h
	Autoclaved-Aerated concrete panel	62.7 ° C	49.2 ° C	1.9 km/h
	PVC-Coated polyester fabric	66.0 ° C	49.7 ° C	2.0 km/h
(10 km/h) Windward	Glassfibre reinforced concrete panel	63.0 ° C	49.2 ° C	2.8 km/h
	Aluminium	63.1 ° C	49.3 ° C	2.7 km/h
	Autoclaved-Aerated concrete panel	60.3 ° C	48.7 ° C	2.7 km/h
	PVC-Coated polyester fabric	63.1 ° C	49.3 ° C	2.7 km/h
(20 km/h) Windward	Glassfibre reinforced concrete panel	58.6 ° C	48.0 ° C	5.1 km/h
	Aluminium	58.7 ° C	48.0 ° C	5.1 km/h
	Autoclaved-Aerated concrete panel	56.7 ° C	47.5 ° C	5.0 km/h
	PVC-Coated polyester fabric	58.7 ° C	48.0 ° C	5.1 km/h

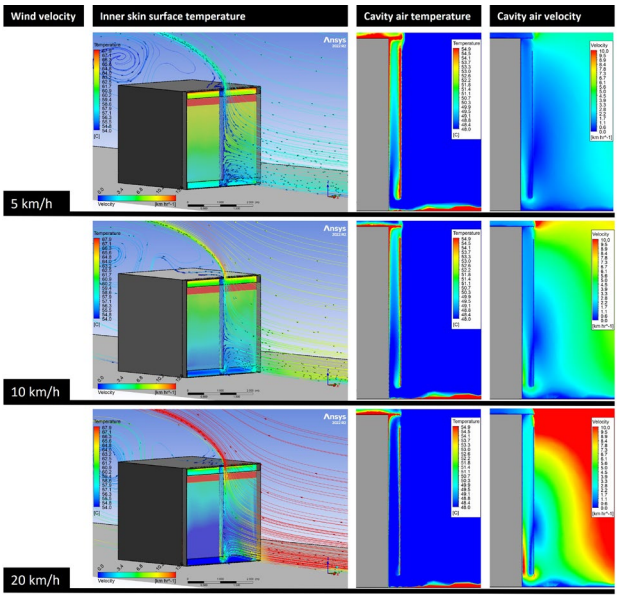

Figure 5: Effect of 5, 10 and 20 km/h wind speeds on the OVF thermal performance.

Table 4 shows CFD simulation results for open and closed joint configurations at 5, 10, and 20 km/h windward of the OVF with an autoclaved-aerated concrete panel outer skin with a 5 cm cavity width. The results show that during a 5 km/h calm breeze, the inner skin surface temperature difference between the open-joint and closed-joint was 2.1ºC. The difference gradually decreases to 0.9ºC during the moderate 20 km/h wind. Therefore, closed-joint OVF showed a better contribution to reducing the inner skin surface temperature as it allowed for air to circulate faster than open-joint OVF.

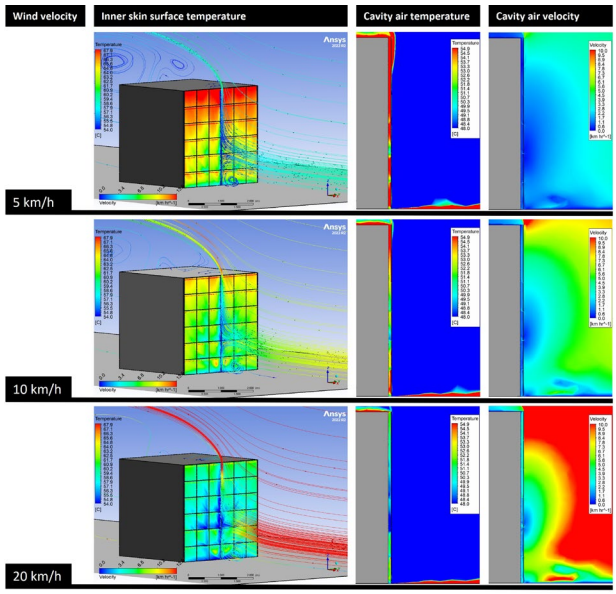

Figure 6: Effect of 5, 10 and 20 km/h wind speeds on the open-joint OVF thermal performance.

Table 4: The CFD simulation results for joints configuration parameter.

Variables		Inner skin temperature	Average air temperature inside the cavity	Average air velocity inside the cavity
Wind velocity	Joint configuration			
(5 km/h)	Open-joint	65.1 ° C	60.1 ° C	1.1 km/h
(10 km/h)		62.4 ° C	56.7 ° C	1.4 km/h
(20 km/h)		58.5 ° C	52.5 ° C	2.4 km/h
(5 km/h)	closed-joint	63.0 ° C	54.3 ° C	2.3 km/h
(10 km/h)		61.2 ° C	52.9 ° C	2.8 km/h
(20 km/h)		57.6 ° C	50.1 ° C	5.1 km/h

The cavity width parameter

A significant finding can be seen in Table 5, where CFD simulations were conducted on four cavity widths with an outer skin made of autoclaved-aerated concrete panels and wind conditions varying from calm to moderate. Also, a graphical comparison is shown in Figure 6 of the effect of 10 km/h wind speed on the thermal performance of 5, 10, 20, and 30 cm cavity widths. The findings indicate that despite the 5 cm cavity having the fastest airflow velocity and the 30 cm cavity having the lowest air temperature inside the cavity, the 5 and 30 cm cases both showed higher inner skin surface temperatures.

This is because in the 5 cm case, the convective heat transfer from the hot outer skin influences the inner skin temperature more since it is closer. In the 30 cm case, the wider cavity caused the airflow speed to slow down, as shown in Figure 7, which is why it caused a higher inner skin surface temperature. Hence, the 10 cm and 20 cm were the most efficient selections because they demonstrated a trade-off between the increase in convective heat transfer from the outer skin in a narrow cavity and the decrease in airflow velocity in a wider cavity.

Table 5: CFD simulation results for the cavity width parameter.

Variables		Inner skin temperature	Average air temperature inside the cavity	Average air velocity inside the cavity
Wind velocity	Cavity width			
(5 km/h) Windward	5 cm	63.0 ° C	54.3 ° C	2.3 km/h
	10 cm	62.4 ° C	50.2 ° C	2.1 km/h
	20 cm	62.7 ° C	49.2 ° C	1.9 km/h
	30 cm	62.9 ° C	49.2 ° C	1.8 km/h
(10 km/h) Windward	5 cm	61.2 ° C	52.9 ° C	2.8 km/h
	10 cm	60.3 ° C	49.2 ° C	2.9 km/h
	20 cm	60.3 ° C	48.7 ° C	2.7 km/h
	30 cm	60.7 ° C	48.6 ° C	2.6 km/h
(20 km/h) Windward	5 cm	57.6 ° C	50.1 ° C	5.1 km/h
	10 cm	56.8 ° C	47.7 ° C	5.1 km/h
	20 cm	56.7 ° C	47.5 ° C	5.0 km/h
	30 cm	57.2 ° C	47.6 ° C	4.8 km/h

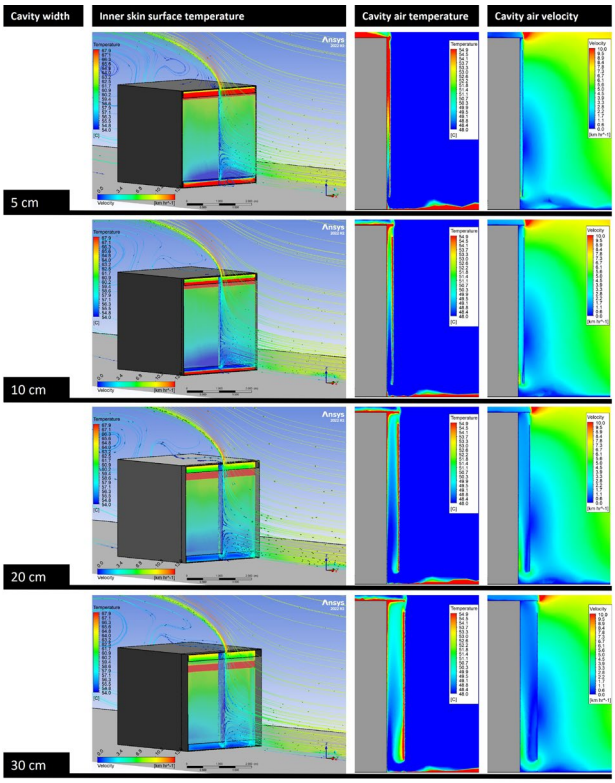

Figure 7: Cavity width parameter comparison of 5, 10, 20 and 30 cm cavities.

The wind direction parameter

The wind direction must be changed when simulating the OVF, as the wind does not always face it. Table 6 illustrates how three wind directions, leeward, windward, and side, affect the temperature of the opaque ventilated façade and the velocity through the cavity. The wind direction parameter was simulated using an autoclaved-aerated concrete panel outer skin with a 20 cm cavity. At all wind speeds, the lowest inner skin surface temperatures could be achieved when the wind faced the ventilated façade. Figure 8 illustrates how airflow streamlines through the cavity in all simulated wind directions influence on its thermal performance. These simulations indicate that the geometrical solution for the OVF found in the literature should be able to respond more efficiently to changes in wind direction.

The solar exposure parameter

The OVF must perform well both when it is exposed to sunlight and when it is shaded, which is why the solar exposure parameter is essential. The autoclaved-aerated concrete panel outer skin with a 20 cm cavity scenario was simulated at three different times of day: 11 a.m. (full sun), 1 pm (partial shaded), and 4 p.m. (fully shaded), and under three different wind speeds, as seen in Table 7. In CFD simulations, shaded OVFs showed significant temperature differences on the inner skin surface. The inner skin temperature difference when the sun faces the ventilated façade at 11:00 a.m. and at 4:00 p.m. was 4.1°C during a calm 5 km/h wind, 3.5°C during a 10 km/h wind, as seen in Figure 9, and 2.7°C during a 20 km/h wind. As a result of these simulations, the geometrical solution for the OVF should allow self-shading of the outer skin, thereby decreasing the amount of heat transmitted.

Table 6: CFD simulation results for the wind direction parameter.

Variables		Inner skin temperature	Average air temperature inside the cavity	Average air velocity inside the cavity
Wind velocity	Wind direction			
(5 km/h)	Leeward	64.5 ° C	52.2 ° C	1.8 km/h
	Windward	62.7 ° C	49.2 ° C	1.9 km/h
	Side	65.3 ° C	52.6 ° C	1.2 km/h
(10 km/h)	Leeward	63.9 ° C	52.9 ° C	2.2 km/h
	Windward	60.3 ° C	48.7 ° C	2.7 km/h
	Side	65.2 ° C	53.0 ° C	1.6 km/h
(20 km/h)	Leeward	61.8 ° C	51.3 ° C	2.5 km/h
	Windward	56.7 ° C	47.5 ° C	5.0 km/h
	Side	63.0 ° C	53.1 ° C	2.7 km/h

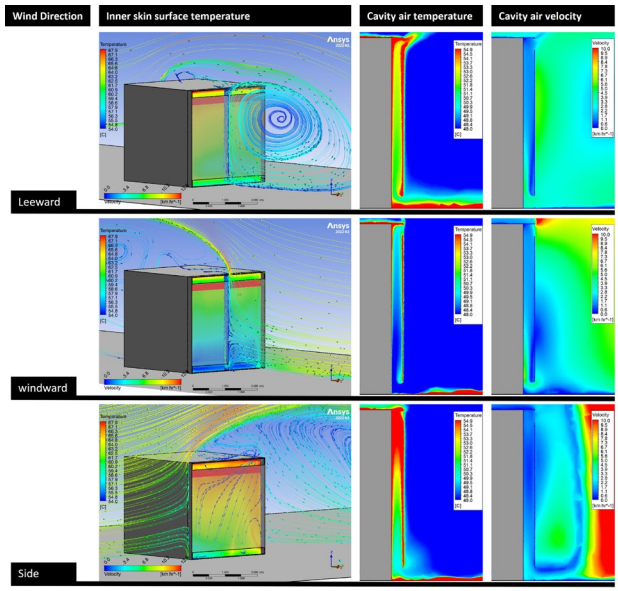

Figure 8: Wind direction parameter comparison during leeward, windward and side directions.

Table 7: CFD simulation results for the solar exposure parameter.

Variables		Inner skin temperature	Average air temperature inside the cavity	Average air velocity inside the cavity
Wind velocity	Solar exposure			
(5 km/h) Windward	Full sun	62.7 ° C	49.2 ° C	1.9 km/h
	Partial shaded	62.0 ° C	49.1 ° C	1.8 km/h
	Fully shaded	58.6 ° C	48.1 ° C	1.7 km/h
(10 km/h) Windward	Full sun	60.3 ° C	48.7 ° C	2.7 km/h
	Partial shaded	59.8 ° C	48.5 ° C	2.6 km/h
	Fully shaded	56.8 ° C	47.5 ° C	2.5 km/h
(20 km/h) Windward	Full sun	56.7 ° C	48.4 ° C	5.0 km/h
	Partial shaded	56.3 ° C	47.3 ° C	5.0 km/h
	Fully shaded	54.0 ° C	46.7 ° C	5.0 km/h

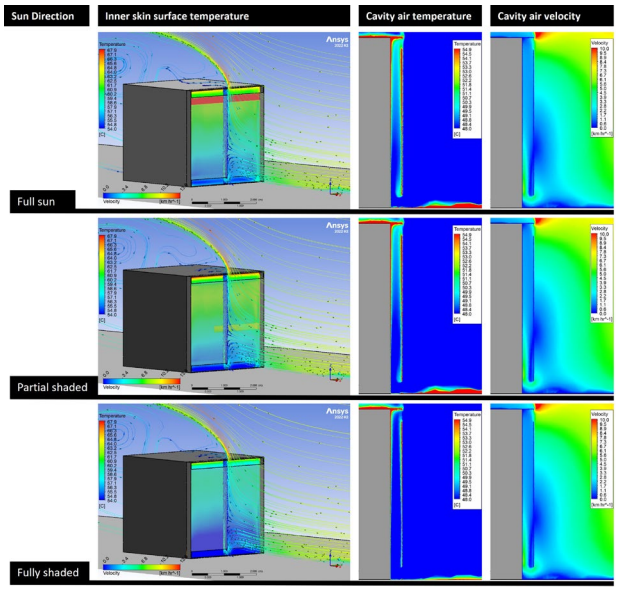

Figure 9: Solar exposure parameter comparison during a 10 km/h light wind.

Conclusion

The purpose of this paper is to present a baseline design of an OVF in a hot arid climate using CFD simulations to evaluate the characteristics discovered in the literature review that affect its performance. An optimisation study of the baseline façade will be performed in the future to compare its performance with the baseline façade. Several design parameters affecting ventilated façades were examined in depth, including outer skin materials, joints configuration, air cavity width, wind direction and velocity, and solar exposure. As a result of the study, the following significant results were found:

- For the outer skin, the autoclaved-aerated concrete panel reduced surfaces and air temperatures more effectively.
- CFD simulations of four cavity widths found that the 10 cm and 20 cm cavities almost had equal impacts on inner skin surface temperatures. While the 5 cm and 30 cm cavities cause higher inner skin surface temperatures.
- The lowest inner skin surface temperature can be achieved regardless of the wind speed when the wind faces a ventilated façade.
- The geometrical solution for the OVF should allow for self-shading of the outer skin, thus reducing heat transmission.

For an optimum OVF design, the cavity design must boost airflow velocity because the baseline model's ventilated cavity geometry reduces the average airflow inside the cavity by about 70% compared to the wind speed. As an example, the maximum average air velocity inside the cavity was 2.9 km/h during a 10 km/h light wind. Furthermore, the outer skin of the OVF should minimise sun irradiance and maximise shadowed areas. This study's most important findings will guide the development and testing of additional OVF designs. This approach can provide researchers with the opportunity to examine a variety of OVF designs and determine which parameters should be prioritised in the creation of a novel OVF in hot and arid climates.

References

ANSYS. (2022). *ANSYS Fluent User's Guide*.

Astorqui, J., & Porras-Amores, C. (2017). Ventilated Façade with double chamber and flow control device. *Energy and Buildings*, *149*.

Balocco, C. (2002). A simple model to study ventilated facades energy performance. *Energy and Buildings*, *34*(5), 469–475.

Buratti, C., Palladino, D., Moretti, E., & Palma, R. Di. (2018). Development and optimization of a new ventilated brick wall: CFD analysis and experimental validation. In *Energy and Buildings* (Vol. 168, pp. 284–297).

C. O. Souza, L., A. Souza, H., & F. Rodrigues, E. (2018). Experimental and numerical analysis of a naturally ventilated double-skin façade. *Energy and Buildings*, *165*, 328–339.

Castillo, J. A., Huelsz, G., van Hooff, T., & Blocken, B. (2019). Natural ventilation of an isolated generic building with a windward window and different windexchangers: CFD validation, sensitivity study and performance analysis. *Building Simulation*, *12*(3), 475–488.

Ciampi, G., Spanodimitriou, Y., Scorpio, M., Rosato, A., & Sibilio, S. (2021). Energy performance of PVC-Coated polyester fabric as novel material for the building envelope: Model validation and a refurbishment case study. *Journal of Building Engineering*, *41*, 102437.

Ciampi, M., Leccese, F., & Tuoni, G. (2003). Ventilated facades energy performance in summer cooling of buildings. *Solar Energy*, *75*(6), 491–502.

Coma, J., Pérez, G., de Gracia, A., Burés, S., Urrestarazu, M., & Cabeza, L. F. (2017). Vertical greenery systems for energy savings in buildings: A comparative study between green walls and green facades. *Building and Environment*, *111*, 228–237.

Fantucci, S., Serra, V., & Carbonaro, C. (2020). An experimental sensitivity analysis on the summer thermal performance of an Opaque Ventilated Façade. In *Energy and Buildings* (Vol. 225).

Ferziger, J. H., Perić, M., & Street, R. L. (2020). *Computational Methods for Fluid Dynamics* (4th ed. 20). Springer International Publishing.

Gagliano, A., & Aneli, S. (2020). Analysis of the energy performance of an Opaque Ventilated Façade under winter and summer weather conditions. *Solar Energy*, *205*, 531–544.

Gagliano, A., Nocera, F., & Aneli, S. (2016). Thermodynamic analysis of ventilated façades under different wind conditions in summer period. *Energy and Buildings*, *122*, 131–139.

Gray, D. D., & Giorgini, A. (1976). The validity of the boussinesq approximation for liquids and gases. *International Journal of Heat and Mass Transfer*, *19*(5), 545–551.

Hu, H. H. (2012). *Chapter 10 - Computational Fluid Dynamics* (P. K. Kundu, I. M. Cohen, & D. R. B. T.-F. M. (Fifth E. Dowling (eds.); pp. 421–472). Academic Press.

Ibañez-Puy, M., Vidaurre-Arbizu, M., Sacristán-Fernández, J. A., & Martín-Gómez, C. (2017). Opaque Ventilated Façades: Thermal and energy performance review. *Renewable and Sustainable Energy Reviews*, *79*(February), 180–191.

Lai, C. M., & Hokoi, S. (2017). Experimental and numerical studies on the thermal performance of ventilated BIPV curtain walls. *Indoor and Built Environment*, *26*(9), 1243–1256.

Maciel, A. C. F., & Carvalho, M. T. (2019). Operational energy of opaque ventilated façades in Brazil. *Journal of Building Engineering*, *25*, 100775.

McLean, D. (2013). *Understanding aerodynamics arguing from the real physics* (1st editio). Wiley.

Nghana, B., Tariku, F., & Bitsuamlak, G. (2021). Assessing ventilation cavity design impact on the energy performance of rainscreen wall assemblies: A CFD study. *Building and Environment*, *196*, 107789.

Pasut, W., & De Carli, M. (2012). Evaluation of various CFD modelling strategies in predicting airflow and temperature in a naturally ventilated double skin façade. *Applied Thermal Engineering*, *37*, 267–274.

Rieder. (2017). *concrete skin Characteristics*.

Salim, S. M., & Cheah, S. C. (2009). Wall y+ Strategy for Dealing with Wall-bounded Turbulent Flows. In *Lecture Notes in Engineering and Computer Science* (Vol. 2175).

Sánchez, M. N., Giancola, E., Blanco, E., Soutullo, S., & Suárez, M. J. (2020). Experimental Validation of a Numerical Model of a Ventilated Façade with Horizontal and Vertical Open Joints. In *Energies* (Vol. 13, Issue 1).

Sanjuan, C., Suárez, M. J., González, M., Pistono, J., & Blanco, E. (2011). Energy performance of an open-joint ventilated façade compared with a conventional sealed cavity façade. In *Solar Energy* (Vol. 85, Issue 9, pp. 1851–1863).

Sarihi, S., Mehdizadeh Saradj, F., & Faizi, M. (2021). A Critical Review of Façade Retrofit Measures for Minimizing Heating and Cooling Demand in Existing Buildings. *Sustainable Cities and Society*, *64*, 102525.

Schabowicz, K., & Zawiślak, Ł. (2020). Numerical Comparison of Thermal Behaviour Between Ventilated Facades. *Studia Geotechnica et Mechanica*, *42*.

Schabowicz, K., Zawiślak, Ł., & Staniów, P. (2021). Efficiency of ventilated facades in terms of airflow in the air gap. *Studia Geotechnica et Mechanica*, *43*(3), 224–236.

Sotelo-Salas, C., Esparza López, C. J., & Escobar del Pozo, C. (2019). Comportamiento Térmico de fachada ventilada opaca en clima cálido seco extremo. *Revista de Arquitectura y Diseño*, 20–28.

Sotelo-Salas, C., Pozo, C. E. del, & Esparza-López, C. J. (2021). Thermal assessment of spray evaporative cooling in opaque double skin facade for cooling load reduction in hot arid climate. In *Journal of Building Engineering* (Vol. 38).

Stavrakakis, G. M., Koukou, M. K., Vrachopoulos, M. G., & Markatos, N. C. (2008). Natural cross-ventilation in buildings: Building-scale experiments, numerical simulation and thermal comfort evaluation. *Energy and Buildings*, *40*(9), 1666–1681.

Teodosiu, C., Kuznik, F., & Teodosiu, R. (2014). CFD modeling of buoyancy driven cavities with internal heat source—Application to heated rooms. *Energy and Buildings*, *68*, 403–411.

Yakhot, V., & Orszag, S. A. (1986). Renormalization group analysis of turbulence. I. Basic theory. *Journal of Scientific Computing*, *1*(1), 3–51.